Development of an iron ore sinter process model to predict sinter strand operating parameters using the finite difference method

J. Muller, T.L. de Vries, B.A. Dippenaar, and J.C. Vreugdenburg
Kumba Iron Ore, Anglo American plc

Iron ore fines are agglomerated in the sintering process to produce sinter: an important feed material for blast furnaces worldwide. A model of the iron ore sintering process has been developed with the objective of being representative of the sinter pot test, the standard laboratory process in which the behaviour of specific sinter feed mixtures is evaluated. The model aims to predict sinter quality, including chemical quality and physical strength, as well as key sinter process performance parameters such as production rate and fuel consumption rate. The model uses the finite difference method (FDM) to solve heat and mass distributions within the sinter pot over the sinter bed height and time dimensions. This method can further be used for establishing empirical relationships with measured sinter properties. Inputs into the model include the feed material physical properties, chemical compositions, and boundary conditions that vary over time. Sub-models describe relationships between applied pressure differential and gas flow rate through the bed of granulated fine ore particles, combustion of carbonaceous material, calcination of fluxes, evaporation and condensation of water, and melting and solidification. Four sinter pot tests were performed and the model predictions validated against temperatures measured at depths of 100, 230, and 420 mm. Differences between predicted and measured temperatures indicated the need for optimization of some model parameters that are uncertain. Optimization resulted in an improvement in the correlation between the predicted and measured temperatures for all tests, although an acceptable level of agreement was not achieved in all cases. Using these parameter values, reasonable agreement was found in terms of typical performance parameters for three out of the four tests.

Keywords: iron ore sintering, finite difference method, coke combustion, calcination, evaporation and condensation, melting and solidification, sinter strength.

Introduction

The depletion of high-grade iron ore resources worldwide has led to the situation where finer iron ore products have to be utilized in order to achieve an adequate Fe product grade. In order to utilize this fine material in the blast furnace (which is the ironmaking process used by about 90% of the world's steelmakers), agglomeration in some form becomes essential. Of the available techniques, sintering is by far the most common and usually the most cost-effective process. In recent years, developments in sintering have made it possible for sinter plants to include up to about 30% iron ore concentrate in the Fe raw material mix. Thus the sintering process seems likely to retain its dominant position in terms of agglomeration of iron ore fines for blast furnace feed.

Research and development for the sintering process on the laboratory or pilot scale is typically conducted by means of a sinter pot test. The VIU (value-in-use) team at Kumba Iron Ore routinely uses sinter pot tests to evaluate the performance of new sinter raw materials, investigate optimum sinter blends or the impact of changes in sinter blends, and to provide information for our customers on maximizing the performance advantages and managing any disadvantages of our fine ores in sinter blends. As such, the VIU sinter pot test equipment is in high demand.

The first problem with this is that sinter pot tests are time-consuming, thus the turnaround time can be slow. Secondly, the tests are also very costly. For the above reasons, it is clear that a modelling tool that could predict the key outcomes of sinter tests with a reasonable level of accuracy in would be valuable for assessing the viability of a certain sinter blend in the initial phases of a project. It is not expected that the model could replace the pot test, but that it would complement the pot test work and possibly reduce the number of actual tests required.

This paper discusses the work done to date towards this goal. This includes the development of the model and the testing, optimization, and validation work that has been completed by the authors at the time of publication.

The sinter pot test

The assumption of this test is that the continuous industrial sintering belt process can be adequately approximated by using a batch 'pot' test (almost like a belt cut) in which the material contained in the stationary sinter pot passes through the same process stages as the material would on a sinter belt. The sinter pot test flow diagram is illustrated in Figure 1.

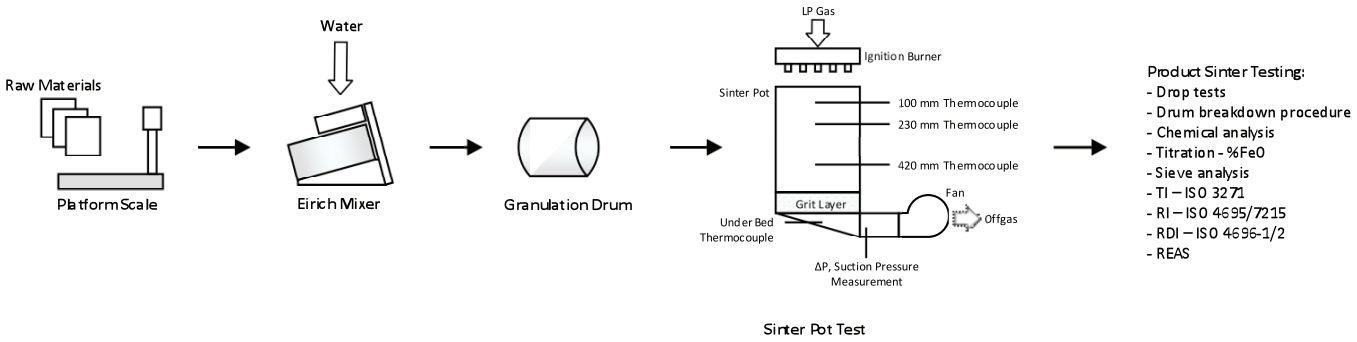

Figure 1. Illustration of the sinter pot test flow sheet

The sinter pot test procedure is as follows. After the equipment is prepared, the raw material blend is manually weighed and fed into the test pot via a primary (Eirich) mixer and a granulation drum. Once the pot has been filled, key settings, including the ignition time and temperature and the pressure drop set-points of the various stages, are entered on the sinter control system via the SCADA interface. Typically, the applied pressure differential below the pot is pressure-controlled rather than flow rate controlled, and the material in the pot is ignited using LP gas.

Ignition is commenced by the operator and the ignition hood is moved into position above the pot. The flame intensity is increased by opening the air supply valve completely, and the ignition temperature is manually controlled by the operators by regulating the gas flow. The ignition stage ends automatically after the prescribed time has elapsed and the process proceeds to the sintering stage. The end of sintering is defined as the time at which the peak exhaust gas temperature is measured, indicating that the flame front has travelled all the way through the sinter cake. An optional cooling cycle may be included after this, where cold air continues to be drawn through the sinter cake. However, this is used only occasionally.

After sintering is completed, the sinter cake is removed from the pot using an overhead crane and then proceeds to physical and metallurgical testing. This starts with a set of drop tests followed by a drum breakdown procedure; after which the sample is screened to determine the size distribution of the final sinter. The FeO content of the sample is measured by titration, and the following additional tests are conducted: a TI (Tumble Index) test as per ISO 3271, a RI (Reducibility Index) test as per ISO 4695 and ISO 7215, and a RDI (Reduction Disintegration) test as per ISO 4696-1 and ISO 4696-2. If required, REAS (Reduktion, Erweichung, und Abschmelzen – meaning reduction, softening, and melting) tests are also carried out to determine the softening and melting characteristics of the sinter.

The performance of a sinter in the pot test is defined by several measures, including productivity, fuel rate, and the strength and reactivity of the sinter as defined by the physical and metallurgical tests listed above. In order for a sinter model to be useful to VIU, it ultimately needs to be able to predict all of these parameters with a reasonable degree of accuracy. In order to calibrate and validate the VIU sinter model, four special sinter pot tests were conducted in which additional thermocouples were mounted in the pot at various depths so that the measured temperature profiles in the sinter cake recorded during the test could be compared with those predicted by the model. Thermocouples were inserted to depths of 100 mm, 230 mm, and 420 mm, measured from the top of the sinter pot.

Sinter modelling

General principles

The sinter pot test can be simulated by modelling the mass and heat transfer phenomena occurring within the sinter bed over time as the boundary conditions change. Chemical reactions, heat transfer, and physical transformation can be modelled, and the temperature profiles, chemical compositions, gas flow velocities, etc. predicted. Physical strength

parameters of the final sinter can be estimated through correlations with some of these predicted variables. Previous researchers have developed several such models describing iron ore sintering with various degrees of complexity (Dash *et al*., 1974; Thurlby, 1988; Patisson *et al*., 1991; Clixby and Young, 1992; Yang *et al*., 2004; Majumder *et al*., 2009). More recently Zhou *et al*. (2012a) also reported on the development of such a model, and evaluated such work currently available in the literature (Zhou *et al*., 2012b).

The sinter pot test itself can be seen as a transient 3D (three-dimensional) problem. However, mass and energy parameters vary predominantly in the height dimension, as well as over time as the flame front travels downwards through the sinter bed. Variations in the other two dimensions (across the diameter to the sides of the sinter pot and effects at the sides of the sinter bed) are relatively small. This simplification is also applicable when this material volume is viewed as part of the sinter strand.

The sinter pot test is modelled here according to a transient 1D approach, illustrated in Figure 2. The transformation of a 1D section of solid material (control volume) from the sinter bed (Figure 2a), which includes a returned (recycled) sinter fines layer at the bottom (grit), is modelled over time. Gas flow in the model is from the top to bottom of this 'control volume'. The solids temperature and chemical composition profiles are modelled over time, as well as the change in temperature and chemical composition of the gas flowing from top to bottom. The variable profiles along the sinter bed height (*e.g*. solids temperature, shown in Figure 2a) are combined for all of the time steps simulated to produce an illustration such as Figure 2b, showing solids temperature. This illustrates the complete sinter process from start to finish, representative of the 'control volume' of material, which moves at the speed of the sinter strand. Variables may also be illustrated over time and at a specific depth, for example, the solids temperature as shown in Figure 2c.

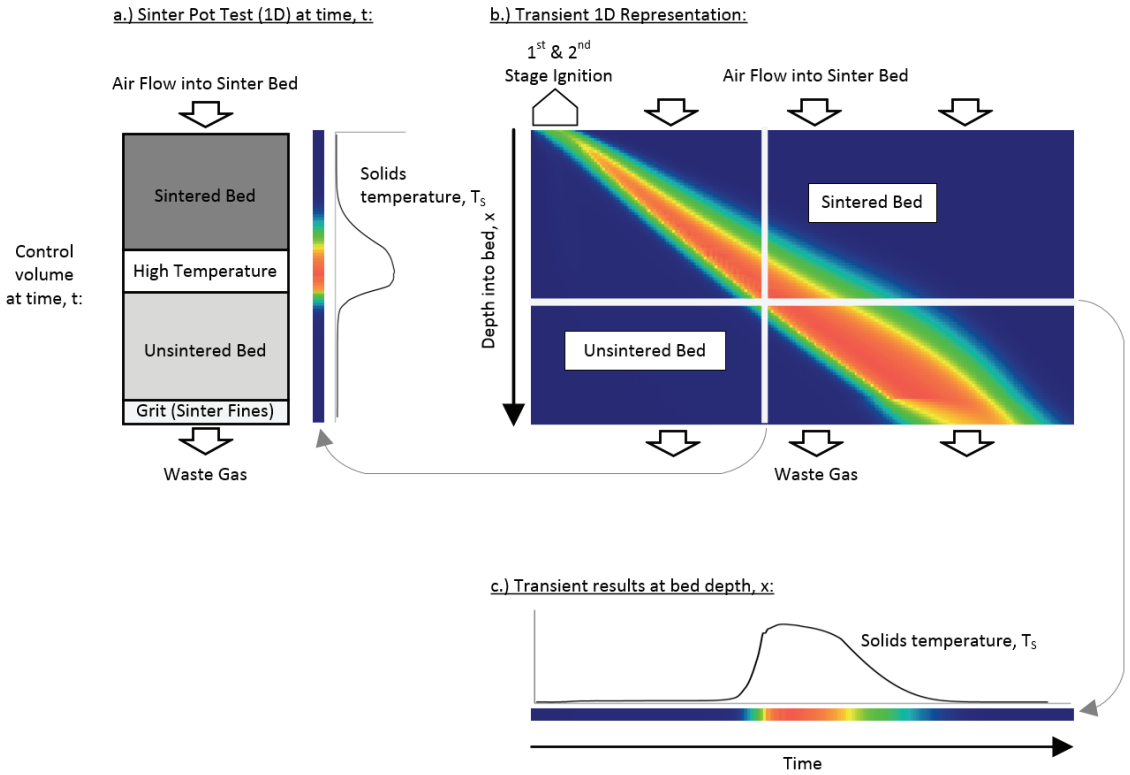

Figure 2. Illustration of the 1D transient sintering process model

Model inputs

Initial and boundary conditions that have to be specified as inputs to the model include the following:

- *Individual feed materials specification* (*e.g*. each ore, flux, fuel, etc.): amount of each constituent in feed mixture (recipe), chemical composition, particle size distribution, physical properties (density, porosity)
- *Granulated feed material (mixed feed to the sinter pot) and bottom grit layer specification*: particle size distribution, void fraction (or JPU to use for estimating void fraction), and sphericity
- *Sinter product requirement*: basicity (CaO/SiO_2), and percentages of FeO, MgO, and SiO_2 (optional)

- *Sinter process/boundary conditions*: bed and grit layer heights, ignition duration, ignition gas temperature, chemical composition, pressure at top of bed, and applied pressure differential below bed (for first and second ignition stages, and then normal sintering)
- *Simulation controls*: number of height elements, duration of time step, simulation maximum time, iterative calculation controls, sub-model control parameters, and results derivation parameters (*e.g.* sintering time defining temperature).

The amounts of ores, fuels, return fines, burnt lime, and moisture are specified in terms of the ratios making up the granulated feed. The amounts of other fluxes (dolomite, silica, lime) are determined for the feed blend prior to model calculation, in order to achieve the required sinter product basicity (CaO/SiO_2) and percentages of MgO and SiO_2.

As it is difficult to measure or derive the feed material void fraction accurately, allowance is made in the model for it to be estimated from a measured JPU (Japanese Permeability Unit), because this parameter is often measured for the actual granulated sinter feed material. The actual pressure drop over the standardized JPU test sample is calculated using Equation [1] (Lwamba and Garbers-Craig, 2008). The material void fraction is iteratively determined using the Ergun equation (Equation [2]) with the other physical material properties of the sinter feed.

$$JPU = \frac{V}{A\left(\frac{H}{\Delta P}\right)^{0.6}} \quad [1]$$

where is the pressure drop over the sample (mm H_2O), H the sample height over which pressure drop is measured (mm), he gas flow rate ($Nm^3.min^{-1}$), and A the sample area (m^2) (Lwamba and Garbers-Craig, 2008).

Model solution

The finite difference method (FDM) has been used to solve transient mass and energy conservation equations. The modelling approach followed and software algorithm are in principle the same as what is described in more detail elsewhere (Majumder *et al.*, 2009). An overview of the method is provided here, but for brevity the conservation- and other model equations have not been repeated in this paper, unless they were different to those used in previous studies (Majumder *et al.*, 2009) or of specific importance as stated later.

The control volume (illustrated in Figure2a) is divided into collections of elements representing gas and solid separately. Variables defined for each element include temperature, chemical composition, reaction rates, etc. For solid elements, the liquid fraction is also defined as a variable, whereas for the gaseous elements, variables are also defined for velocity and pressure.

The combustion of carbonaceous material with oxygen from the air drawn in at the top of the sinter bed primarily determines the amount of heat generated, causing melting of solid phases and therefore forming the basis of the sintering process. The air flow velocity is controlled by the applied pressure differential at the bottom of the sinter bed, and is influenced by the physical properties of the solids, and by heat transfer and the chemical reactions occurring. The model iteratively determines the mass flow rate of gas drawn into the sinter at each simulated time step (Figure 2a). The gas-solid heat and mass transfer is calculated in each element by moving from the top to bottom and using sub-models to describe physical phenomena. After calculation of all the sub-models and the resulting heat and mass transfer between the solids and gas, the pressure drop is calculated over each solid material element, and the air flow rate into the bed adjusted until the total calculated pressure drop converges to that specified as the model input. The pressure drop is calculated as follows using the Ergun equation (after Majumder *et al.*, 2009:

$$\frac{\Delta P}{L} = 150\frac{\mu(1-\varepsilon)^2}{\phi^2 d_p^2 \varepsilon^3} + 1.75\frac{\rho(1-\varepsilon)}{\phi d_p \varepsilon^3}U^2 \quad [2]$$

where is pressure drop over the sample (Pa), L the sample height over which pressure drop is measured (m), μ_g the gas viscosity (Pa.s), ε the bed void fraction, the particle sphericity, d_p the mean particle diameter (m), U the gas velocity ($m.s^{-1}$), and ρ the gas density ($kg.m^{-3}$).

Another important aspect of the energy balance calculated in each element is the assumptions made with respect to the heat of reaction from chemical reactions. Solid and/or gas phase species react with each other to yield products that are also in either the solid and/or gas phase (*e.g.* Equation [3]). In the energy balance of the model, the heat of reaction is split between the enthalpies of the solid and gas products (as per Yang *et al.*, 2004). For each of the chemical reactions identified, a fraction y_i is specified as the fraction of the heat distributed to the gas, with the balance to the solids. For the chemical reactions the model parameters are defined as important model inputs that greatly affect the predicted temperature profiles – y_{dol} dolomite calcination; y_{comb}: coke combustion; y_{ecap}: evaporation; y_{cond}: condensation.

$$A(s) + B(g) \rightarrow C(s) + D(g) \quad [3]$$

Sub-models

Sub-models are formulated to model the gas-solids heat transfer and mass transfer due predominantly to chemical reactions as the gas enters at the top and moves through the sinter bed. Convective heat transfer between gas and solids is modelled only, with conduction and radiation excluded for simplification. Depending on the nature of the chemical reactions, heat is generated or consumed by the chemical reactions and distributed between the resulting gas and solid phases. Chemical reactions are modelled for water evaporation and condensation, dolomite calcination, coke combustion, and melting and solidification of all materials, including Fe raw materials. Physical transformation of the solids, *e.g.* bed shrinkage, is not modelled here for purposes of simplification, but could be included as part of future improvements to the model. Details on each sub-model as implemented here are provided below.

Convective heat transfer

Heat transfer between the downward-moving gas and solids particles in the sinter bed occurs mostly by means of forced convection. Heat transfer rate is calculated in each finite element from the relevant solid and gas temperatures, and a modelled heat transfer coefficient, h_{gs} (as per models by Majumder *et al.*, 2009 and Pattison *et al.*, 1991). This is a function of the incoming gas velocity, density and heat capacity, the sinter bed solids void fraction, and the channeling length factor, ξ. The latter factor (according to Pattison *et al.*, 1991) is used to consider the size of the sinter bed aggregate relative to its constituent particles The sensitivity of the model to this parameter has been evaluated, as reported in a subsequent section.

Water evaporation and condensation

Water evaporates from the wet granulated feed in the warmer areas of the sinter bed around where the flame front progresses downwards through the sinter bed. As the gas flows through the unsintered bed, it carries this water vapour downwards into cooler areas of the bed below the flame front, where condensation becomes possible.

The rates at which evaporation (drying) or condensation occurs in each solids element are estimated using the model reported by Patisson *et al.* (1990). Firstly, the mass transfer rate in the gas boundary layer is modelled as a function of the gas temperature and pressure, the gas-solid heat transfer coefficient, and the logarithmic mean of the actual and saturated molar fractions of moisture in the gas phase (Patisson *et al.*, 1990). This is then used to model the rate of moisture transfer between the gas and solids phases, and is also dependent on the specific area of the solids and the actual and saturation H_2O partial pressures in the gas phase. Condensation is thus considered to occur at a constant rate, independent of the amount of moisture in the solids. Evaporation, however, is modelled to start decreasing from this rate after a critical solids moisture content has been reached (Patisson *et al.*, 1990). A critical moisture content of 5% was used here (as per Majumder *et al.*, 2009).

Limestone and dolomite calcination

$CaCO_3$ and $MgCO_3$ are present in some of the sinter feed materials, typically dolomite and lime. These species start to decompose at a certain temperature in the sintering process, enriching the gas with CO_2. The decomposition rate is modelled separately for $CaCO_3$ and $MgCO_3$ in each solids finite element using simple rate equations as functions of the solids temperature at that point (as per Thurlby, 1988).

Coke combustion

Coke (and possibly other carbonaceous materials) is added to the sinter feed mixture as the fuel source, with the carbon reacting with oxygen to produce CO and CO_2 and generating the heat required to initiate melting of the solids and assimilation of the remaining particles. Sinter models reported in the literature apply different combustion models, which also consider the generation and further combustion of CO, as well as the Boudouard reaction whereby CO_2 is converted back to CO. Here the combustion model by Gibb and Field has been applied (as per Mei *et al.*, 2010). In this approach the above combustion reactions are combined as follows, where the degree of oxidation is represented by the parameter ϕ:

$$\phi C + O_2 \rightarrow 2(\phi - 1)CO + (2 - \phi)CO_2 \quad [4]$$

The parameter ϕ is modelled as a function of temperature (Equation [5]). At lower temperatures, CO_2 is predicted as the main product, while at higher temperatures (from around 1000 K) mostly CO is predicted as the Boudouard reaction is predominant (Zhou, 2012a).

$$\frac{2(\phi - 1)}{2 - \phi} = A_s \exp\left(-\frac{T_s}{T_p} \right) \quad [5]$$

where T_p is the particulate (solids) temperature (K), and A_s and T_s are model parameters with values of 2500 K and 6240 K respectively, as suggested by Mei *et al*. (2010). The sensitivity of the model results with respect to these two model parameters is discussed later.

The carbon reaction rate is limited by the diffusion rate of oxygen to the reaction surface through a stagnant boundary layer. The reaction rate is calculated as a function of the parameter ϕ and other parameters, including the coke particle physical properties, far field oxygen concentration, external and internal gas diffusion coefficients, and the particle (solids) temperature, with the equation provided by Mei *et al*. (2010).

During the validation of the above model, it was found that the modelled combustion reaction rate needs to be further limited to improve the overall correlation between predicted and measured temperatures. After first evaluating several other combustion sub-models used in sinter models available from the literature, the coke combustion limiting factor, x_{CCLF}, was introduced as the fraction of material that can partake in the combustion reaction. This parameter has a default value of 1.0, which would yield the same results as previously. Reducing the value towards zero decreases the amount of carbon allowed to combust during a time step. Irrespective of the value chosen for this parameter, the same amount of coke is combusted over time if conditions allow combustion to occur. This factor effectively spreads out the heat generation over time and lowers the peak temperatures, widening the temperature curves.

Melting and solidification

Melting and solidification are two of the most important phenomena in sintering, since they enable particle assimilation and directly affect the physical properties of the sinter product. When the fines reach a certain temperature the primary melt forms, with its properties being a function of the temperature achieved and its chemical composition (Debrincat *et al*., 2004). The primary melt chemical composition is in turn influenced by the gradual assimilation of different individual particles into the melt, and subsequently also the bonding phases formed during solidification and the properties of the sinter product, *e.g*. sinter strength and reducibility (Debrincat *et al*., 2004).

This complex process of melting and solidification is simplified firstly by not specifically modelling the rate at which it occurs, based on the implicit assumption that heat transfer is rate limiting (modelled separately). A method by Zhou *et al*. (2012a) is used here to estimate the fraction melted as a function of the solids temperature and chemical composition of the fines fraction:

$$\beta = \left(\frac{T_S - T_{sol}}{T_{liq} - T_{sol}} \right)^{\alpha} \qquad [6]$$

where β is the mass fraction of melted material, T_S is the solids temperature, T_{sol} is the solidus temperature (typically 1100°C, Zhou *et al*., 2012a), and T_{liq} is the liquidus temperature as defined by the chemical composition of the -1 mm fines fraction (typically around 1400°C, Zhou *et al*., 2012a). The value for the phase change factor, α, has been assumed here as unity. The fraction melted, β, would then be unity when the solids temperature is above the liquidus temperature, and the melted fraction would be zero when the solids temperature is below the melting start temperature.

For each solids element in a time step, the fraction melted is derived from the above relationship, with the amount melting or solidifying being the difference from that melted in the previous time step. The heat of melting or solidification is derived and included in the energy balance of each element. A simplified approach is followed in assuming the latent heat of 0.254 MJ/kg for melting, and 0.117 MJ/kg for solidification, as used by Zhou *et al*. (2012a).

Model outputs

The model produces several outputs, which can be used to evaluate overall performance of the sinter mix and predicted sinter product properties with regards to the inputs specified, or to analyse the interrelated phenomena occurring in the sinter bed in order to make process improvements. In future, it may be possible to correlate some calculated model variables with some measured sinter properties, and these relationships may then be included in the model.

The model variables available for each element include:

- *Solids variables*: temperature, and chemical composition (wt.%)
- *Gas variables:* temperature, pressure, chemical composition (vol.%), velocity, and inlet mass flow rate
- *Reaction rates:* evaporation/condensation, limestone and dolomite calcination, and coke combustion reaction rates
- *Other parameters*: heat transfer coefficient, fraction melted and solidified, enclosed area above 200°C and 1100°C (described later, Zhou *et al*., 2012a).

Some of the more important model results calculated (before or after the simulation) are:

- *Bed void fraction:* calculated from the granulated feed material JPU prior to the simulation, to be used then as a model input
- *Coke consumption rate:* coke usage rate calculated as the specified mass of coke feed divided by the calculated mass of sinter produced, with units of kg.t $^{-1}$ sinter

- *Sinter product mass and chemical composition*: calculated from the feed material mixture specification, subtracting ignition loss components (*e.g.* carbon, and carbonates)
- *Sintering time:* indicative of the speed with which the flame front travels through the bed and the sintering rate. Calculated as the time until the bottom of the bed cools to a specified temperature (*e.g.* 150°C)
- *Burn-through times*: similar to the sintering time, but calculated as the time to reach the maximum temperature below the sinter bed
- *Production rate:* rate of sinter produced calculated using the predicted mass of sinter produced and sintering time, typically units of $t.m^{-2}$ per 24 hours
- *Variable averages:* variables (from the above list) averaged over the height of the sinter bed at the end of the simulation.

Model validation and parameter optimization

A stepwise approach was followed to validate the model, and to optimize the values of certain model parameters to improve the correlation between predicted and measured values. Steps included in this process are:

- Conduct four sinter pot tests and gather test data
- Process test data and configure the four models to be representative of tested materials and conditions
- Calculate the four models, using 'standard' model input parameters, as in the referenced literature, and compare predicted solids temperature profiles over time with those actually measured at 100, 230, and 420 mm bed depths
- Investigate the sensitivity of the predicted solids temperature profiles to variation in certain model parameters
- Systematically determine values for these model parameters that yield improved correlations between predicted and measured temperature profiles.

Sinter pot tests and initial model results

Four sinter pot tests were conducted using iron ore fines as primary feedstock to produce data that could be used to validate and improve the model. The feed mixture for test 1 contained no iron ore concentrate, whereas the other mixtures contained around 8% concentrate. The feed material mixtures further varied mostly in terms of percentages of burnt lime and amount of water added for granulation, which affected the permeability of the mixtures (measured in JPU). The most significant differences in the materials used are summarized in Table I, showing the void fraction of the granulated sinter feed, estimated from the measured JPU (Equation [1]).

The parameters reported for each of the four tests include the following (results for all values not provided in this work):

- *Test configuration and process conditions*: parameters required as inputs to the model – individual and granulated feed material specifications, sinter product chemical compositions (using here the actuals obtained), and the process/boundary conditions
- *Measured bed temperatures*: measured with thermocouples over time at depths of 0, 100, 230, and 420 mm, and in the free space under the sinter bed. These temperature measurements generally contain inherent inaccuracies and their reliability varies, which must be taken into account in the analysis of the results (after Loo *et al*., 2012; Zhou *et al*., 2012a)
- *Sintering performance results*: listed in Table II
- *Product sinter properties*: particle size distributions (sieve analyses), chemical compositions, mineralogical compositions (by X-ray diffraction analysis), TI, RDI, and RI.

Table I. Significant properties of materials used as feed for the model validation sinter pot tests

Parameter	Test 1	Test 2	Test 3	Test 4
Iron ore concentrate (wt. %)	0	8.14	8.14	7.79
Burnt lime (wt. %)	0	0	3.7	5.5
Water (wt. %)	5	5.50	6.5	8.2
JPU	27.6	31.3	36.9	43.6
Av. granulated feed particle diameter (mm)	4.23	3.83	4.03	3.91
Feed void fraction (estimated from JPU)	0.28	0.31	0.32	0.35

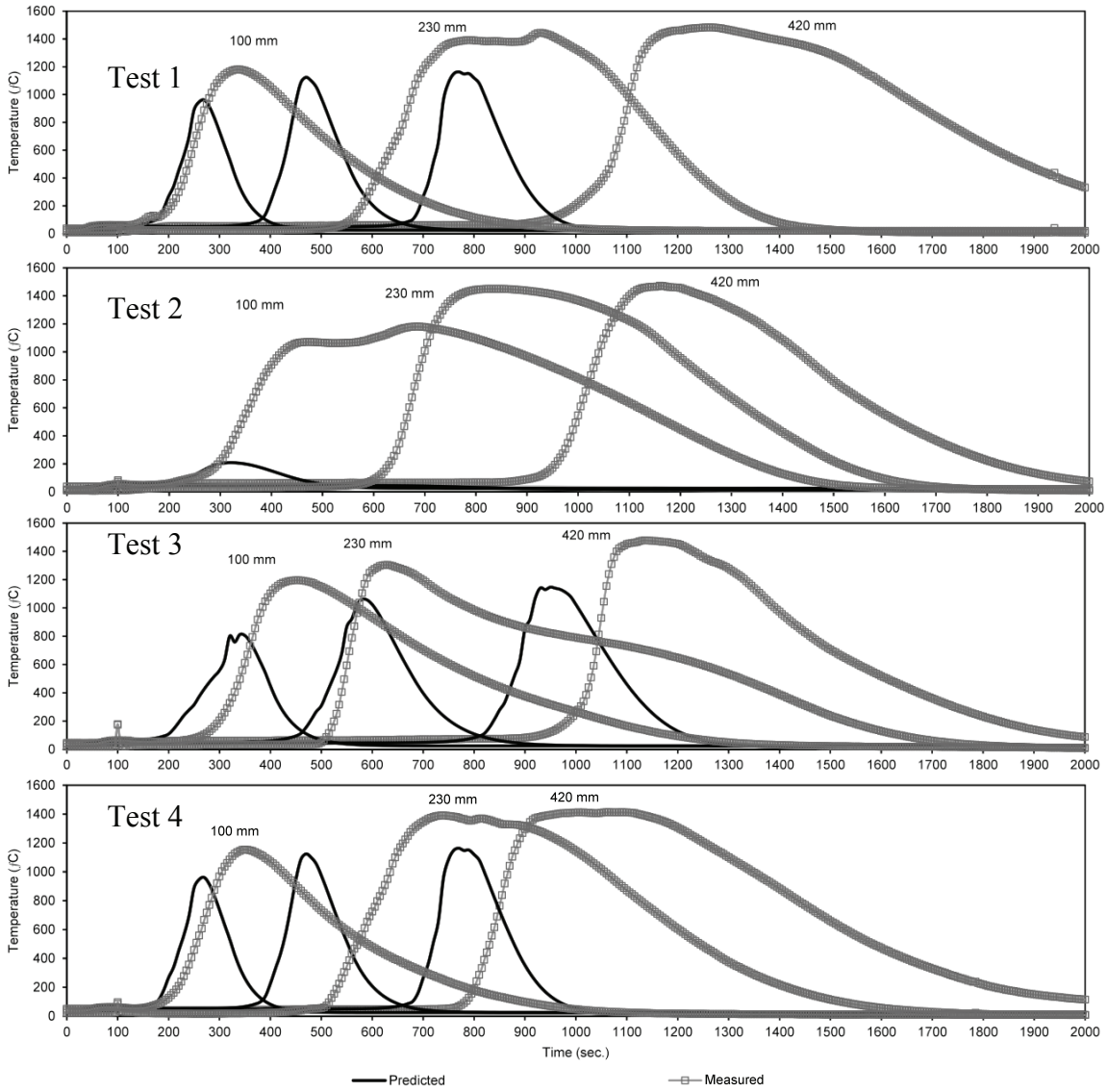

Figure 3. Predicted and measured temperatures at depths of 100, 230, and 420 mm for sinter pot tests 1 to 4 – default model parameter values used

The temperatures that were measured during each of the four sinter pot tests are illustrated in Figure 3. These are shown with model predictions at the same depths in the bed, configuring individual model with values representative of each specific test, and model parameters with default values taken from the literature. The parameters representing the fraction of the heat of reaction to the gas phase, y_i, were all set to zero (*i.e.* all heat of reaction to the solids). For pot test 2, the model predicted that no burn-through would be achieved, hence only a small temperature increase is seen at 100 mm following ignition. For the other pot tests, significant differences exist between predicted and measured temperatures, indicating the need to optimize certain model parameters.

Sintering performance results from the sinter pot tests are listed in Table II. These are calculated from actual measurements of the mass of sinter produced, mass of fuel feed, height of the sinter bed, and the burn-through time (when the peak temperature is measured with the thermocouple in the free space below the bed). The fastest sintering time and highest production rate were obtained for sinter pot test 4. The feed material for this test had the highest JPU (and therefore the highest initial permeability), which resulted in higher gas mass flow rates. The slowest sintering time and lowest production rate were obtained for test 2, despite the material not having the lowest initial permeability, which indicates that sintering is affected by factors other than permeability.

Table II. Sinter process performance results of the four sinter pot tests

Measured parameter	Test 1	Test 2	Test 3	Test 4
Burn-through time (min)	22.2	25.6	21.5	17.9
Burn-through rate (mm.min^{-1})	24.8	21.6	25.6	30.8
Production rate (t sinter per m^{-2}24 h^{-1})	40.4	34.2	38.6	42.2
Fuel consumption rate (kg.t^{-1} sinter)	70.9	68.5	68.1	69.0
Yield (%)	84.5	84.6	86.0	85.8

Model parameter sensitivity

Predicted temperatures deviated significantly from measured temperatures (Figure 3), more so than could be attributed to measurement inaccuracies. This remained largely unchanged when evaluating other sub-models from literature, especially that for coke combustion. For the sinter model to be useful, reasonable agreement is required between predicted and measured temperature profiles. Model parameters with associated uncertainty and with a significant impact on the results were identified, and an attempt was made at improving the overall model accuracy by optimizing their values. The parameters identified are listed in Table III, together with the ranges within which these were evaluated.

Table III. Model parameters optimized to improve correlation between measured and model predicted temperature profiles

Symbol	Description	Range
A_s	Coke combustion model parameter 1 (Equation [5])	1 000 – 300 000
T_s	Coke combustion model parameter 2 (Equation [5])	1 000 – 30 000
y_{comb}	Fraction coke combustion heat of reaction to gas	0 – 1
x_{CCLF}	Coke combustion limiting factor	0 – 1
ξ	Channeling length factor (heat transfer model)	2 – 5

The sensitivities of the predicted solids temperature profiles to these parameters (Table III) were investigated. Figure 4 to Figure 6 illustrate the sensitivities of the model to each of the parameters for sinter pot test 1, by varying one parameter at a time and holding the others fixed at typical values. The solids temperature profiles at 100, 230, and 420 mm are shown for y_{comb} (Figure 4), and only at 230 mm for the other parameters (Figure 5, Figure 6).

These results indicate that the correlation between predicted and measured temperature profiles might be improved by adjusting values of the model parameters identified. Peak temperatures decrease and temperatures rise sooner when y_{comb} is increased (Figure 4), as more heat of combustion is transferred to the gas and is carried downwards to increase the burn-through rate. The temperature peak value and profile width both decrease with A_S, whereas both increase with T_S (Figure 5), as these parameters have opposing effects on the degree of combustion and the amount of heat generated.

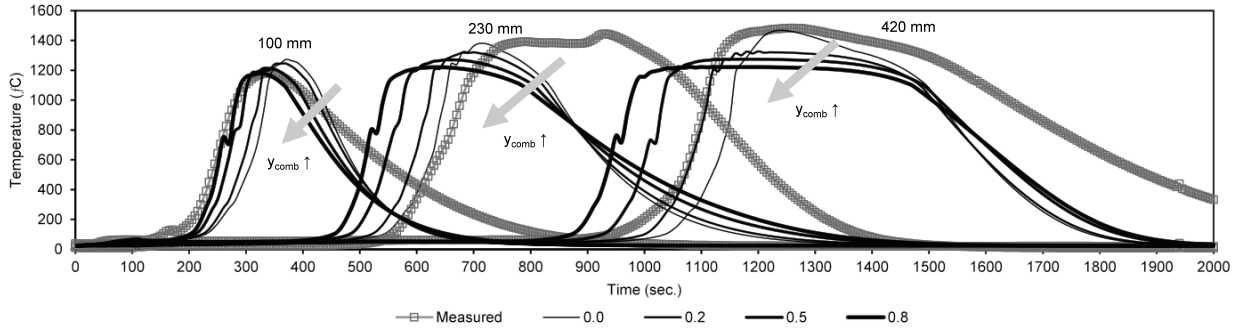

Figure 4. Solids temperature sensitivity (at 100, 230, and 420 mm bed depths) to variations in the fraction of heat of combustion to the gas, y_{comb}. A_S = 2000, T_S = 12 000, x_{CCLF} = 0.2, and ξ = 3

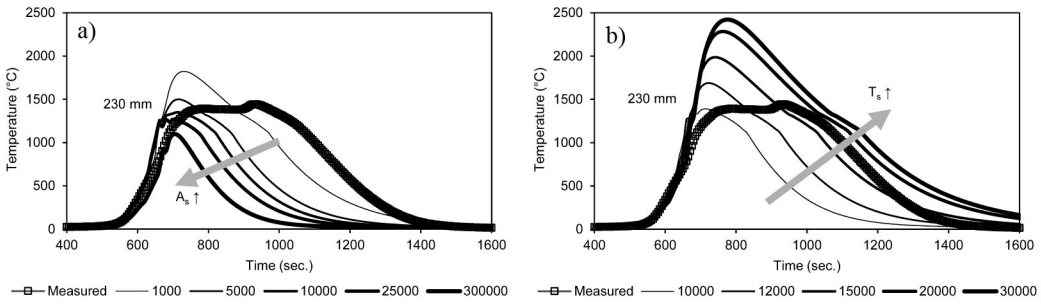

Figure 5. Solids temperature profile sensitivity (at 230 mm bed depth) to variations in coke combustion model parameters. (a) A_S with T_S = 12000, and (b) T_S with A_S = 2000, where y_{comb} = 0, x_{CCLF} = 0.2, and ξ = 3

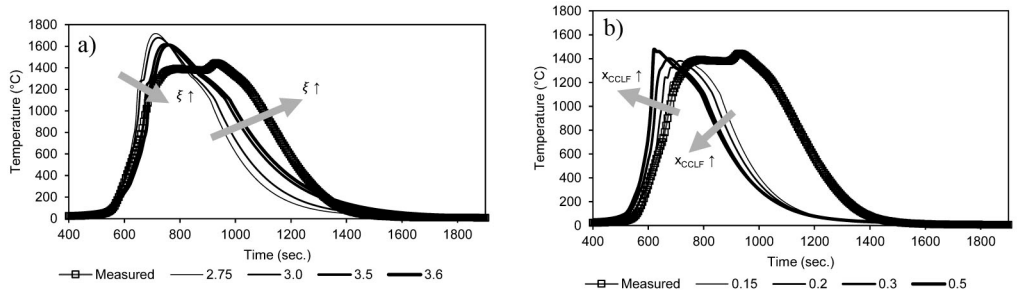

Figure 6 – Solids temperature profile sensitivity (at 230 mm bed depth) to varying (a) the channeling length factor ξ with x_{CCLF} = 0.2, and (b) coke combustion limiting factor x_{CCLF} with ξ = 3. A_S = 2000, T_S = 12000, and y_{coomb} = 0

Sensitivity to is shown to be fairly low (Figure 6a), and due this fact and the narrow range of values for which the model would remain stable, a fixed value of 3 was chosen to be used henceforth to simplify the first round of optimization. Increasing x_{CCLF} causes the temperature to increase sharply to higher peak values (Figure 6a) as more coke is combusted from the time when combustion is predicted to start; with temperatures thereafter decreasing faster as more heat is transferred to the gas.

Model parameter optimization

The model parameter sensitivities in Figure 4 to Figure 6 illustrate the possibility of obtaining improved correlations with measured temperature profiles by adjusting these parameters. Because these parameters have interrelated effects, a systematic approach was used as discussed below to find the optimized values of these model parameters, namely the coke combustion model parameters A_S and T_S, the fraction of combustion heat of reaction to the gas phase y_{comb}, and coke combustion limiting factor x_{CCLF}.

Temperature profile characterization

To optimize the model parameters it is necessary to numerically compare the temperature profiles. The temperature profiles are therefore characterized through a set of parameters derived at each of the depths considered in the test work (100, 230, and 420 mm). The parameters as illustrated in Figure 7 are:

- Maximum solids temperature reached (°C)
- Time to reach the maximum solids temperature from the start of the sintering test (seconds)
- Enclosed area above 200°C (grey colored area illustrated, min.°C) – area under the temperature curve to as low as 200°C (after Zhou *et al.*, 2012a)
- Time to reach temperature of 1100°C (seconds).

Values for the above parameters are derived for the four sinter pot tests using the temperature measurements (Figure 3), listed in Table IV and Table V, and were used as a basis for the model parameter optimization.

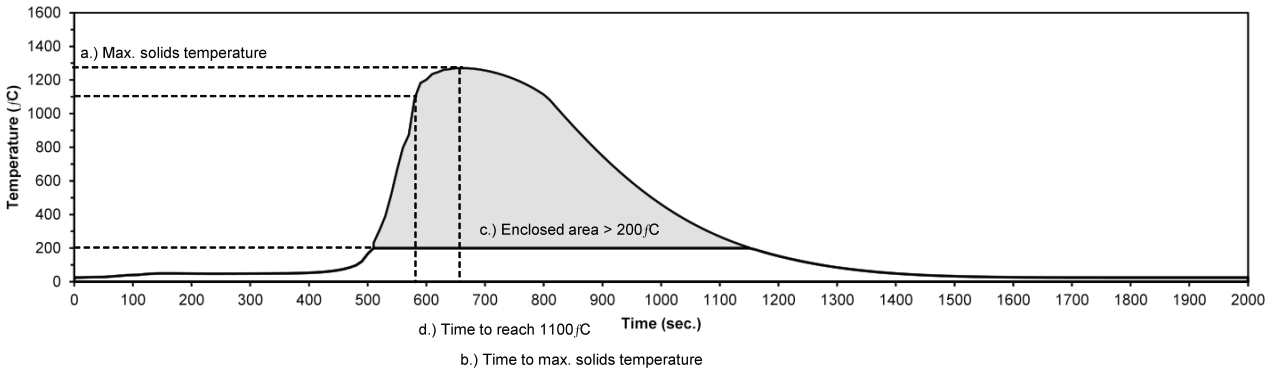

Figure 7. Temperature profile at 230 mm into solids bed showing parameters used to characterize the curve

Table IV. Actual sinter tests maximum solids temperatures and the times to achieve them

Sinter pot test no.	Max. solids temperature at 100 mm (°C)	Max. solids temperature at 230 mm (°C)	Max. solids temperature at 420 mm (°C)	Time to max. solids temperature at 100 mm (s)	Time to max. solids temperature at 230 mm (s)	Time to max. solids temperature at 420 mm (s)
1	1180	1444	1483	335	930	1260
2	1179	1449	1472	680	825	1160
3	1196	1305	1478	450	630	1135
4	1154	1390	1412	350	735	1060

Table V. Actual sinter tests times to 1100°C and enclosed area > 200°C

Sinter pot test no.	Time to 1100°C at 100 mm (s)	Time to 1100°C at 230 mm (s)	Time to 1100°C at 420 mm (s)	Enclosed area > 200 °C at 100 mm (min.°C)	Enclosed area > 200 °C at 230 mm (min.°C)	Enclosed area > 200 °C at 420 mm (min.°C)
1	300	690	1115	4251	13319	13321
2	605	710	1055	10863	11495	9864
3	400	580	1060	6186	9352	9176
4	325	650	875	4216	10255	11871

Calculation of model results for optimization

To find the optimized set of model parameter values that would yield the best correlation between predicted and measured temperature profiles, data had to be generated by calculating the models using possible model parameter values. For each of the model parameters optimized, five values were selected within the range of each considered (Table III). Values were iteratively determined from observing the sensitivity of the model outputs and using smaller intervals in areas of higher sensitivities, with the final values selected listed in Table VI.

Each model configured for one of the sinter pot tests was calculated with all possible combinations of values (Table VI). For the four model parameters with five values each, $5^4 = 625$ value combinations exist, and this was therefore the number of calculations performed with each of the four sinter pot test models.

Table VI. Model parameter values considered for the model parameter optimization

Parameter	Model input values
A_S	1 000, 5 000, 10 000, 25 000, 300 000
T_S	5 000, 10 000, 15 000, 20 000, 30 000
y_{comb}	0, 0.25, 0.75, 1
x_{CLF}	0, 0.1, 0.25, 0.5, 1

After calculation of the all the models, each of the temperature profile characterization parameters (Figure 7) were normalized to an error percentage by comparing the model output with the parameter value measured for the relevant sinter pot test (from Table IV and Table V):

$$e_k = \frac{y_{pred,k} - y_{meas},k}{y_{meas},k} \times 100\% \quad [7]$$

where e_k is the error percentage of relevant output parameter for sinter pot test number k, $y_{pred,k}$ the predicted output parameter value, and y_{meas},k the measured output parameter value (from Table IV and Table V). A normalized error percentage of zero would indicate an output precisely equal to the measured value. These normalized error percentages have only a constrained lower limit, and thus can range from around negative 100% in the worst case. This is typically seen for cases where no burn-through was predicted and the output parameter had a value close to zero.

Model parameter optimization

Results from the above calculations are illustrated for two temperature profile characterization parameters in Figure 8. This shows the dimensionality of the problem, having varied four model parameters, and deriving twelve outputs, only two of which are illustrated for a fixed value of one model parameter (A_S = 25 000). Figure 8 also illustrates the non-linearity of the model, which affects the confidence with which multiple linear regression could be used as an optimization solution.

The results in Figure 8a show that several error percentage lines cross from negative to positive values, and therefore the combinations of the input values for the model predict very closely the measured value (for this parameter). In Figure 8b, however, the lines trend upward towards zero and stabilize without moving into positive values. This could indicate that the value of the parameter not varied here (A_S = 25 000) does not yield a feasible solution and needs to be changed.

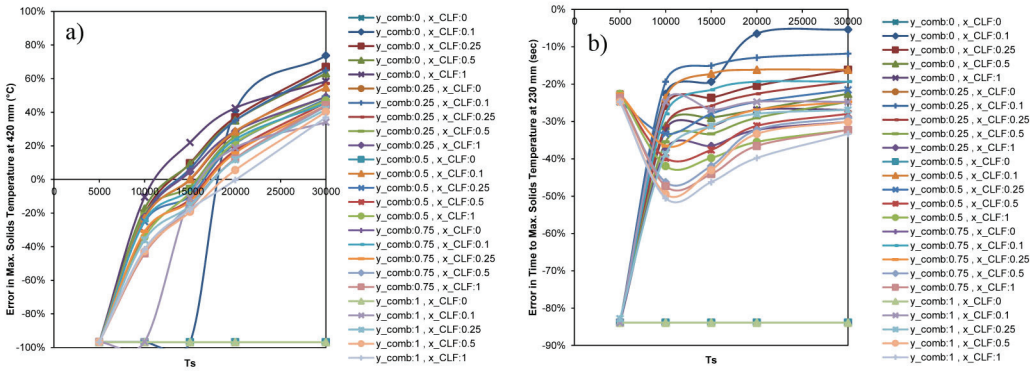

Figure 8. Results of sinter pot test 1 with A_S = 25 000: error percentages of (a) maximum solids temperature at 420 mm, and (b) time to reach the maximum solids temperature at 230 mm

Considering the dimensionality and non-linearity of the problem, 'Kohonen self-organizing maps' (Kohonen, 2001) was chosen as the method to determine the optimum set of model parameter values. This, in short, is an artificial intelligence method that produces a lower dimensional data-set from training data through unsupervised learning. A neighbourhood function is applied to generate regions of data vectors having similar values. This allows finding of the best matching unit (BMU) that has the smallest distance to an input vector using only the selected values specified.

Here the normalized error percentages calculated for each of the four sinter pot tests have been combined into a single data-set and used as training data for the self-organizing map. Each vector of the data-set contained the four model input parameters (normalized between 0 and 1), and the twelve normalized temperature profile characterization error percentages as outputs, representing a single calculation of a model representing any of the four sinter pot tests. The optimized set of model parameter values would ideally be represented by a BMU with all of the twelve outputs having values of zero.

The results from this method are listed in Table VII. Firstly, the BMU was found specifying all outputs as zero, with the resulting BMU vector having significantly larger error percentages for some outputs (>10%). This is likely due to experimental errors, which affected the maximum temperature at 100 mm and all of the temperature profiles at 230 mm in the data-set used. These outputs were then excluded and the values in the last column of Table VII were obtained, with errors of the outputs varying between -5% and +5.3% from those measured.

Table VII. Optimized model parameter values determined using the self-organizing map method (Kohonen, 2001)

Model parameter:	Outputs considered	
	All	**Selected**
A_S	227 382	16 248
T_S	18 663	14582
y_{comb}	0.489	0.417
x_{CCLF}	0.251	0.285
Output errors predicted (%): (target 0%)		
Max. solids temperature at 100 mm	15.7%	-
Max. solids temperature at 230 mm	1.8%	1.0%
Max. solids temperature at 420 mm	-0.1%	-1.5%
Time to max. solids temperature at 100 mm	5.7%	3.8%
Time to max. solids temperature at 230 mm	-27.4%	-
Time to max. solids temperature at 420 mm	-3.8%	-5.0%
Time to 1100°C at 100 mm	1.9%	1.7%
Time to 1100°C at 230 mm	-13.4%	-
Time to 1100°C at 420 mm	-2.7%	-3.3%
Enclosed area > 200°C at 100 mm	-0.8%	-3.7%
Enclosed area > 200°C at 230 mm	-27.0%	-
Enclosed area > 200°C at 420 mm	10.1%	5.3%

The optimized model parameter values, as determined above for the selected set of outputs (last column of Table VII), were applied in the models for each of the four sinter pot tests. The newly predicted temperature profiles are shown as the black lines in Figure 9, together with the measured temperatures, and also (in grey) the temperatures predicted earlier with the default model parameter values (shown in Figure 4).

Reasonable agreement between predicted and measured temperatures has been obtained for test 1, with the exception of the temperatures at 230 mm. For test 2, the predicted profile at 420 mm is acceptable, but with poor correlation at 100 mm. For tests 3 and 4, temperatures are predicted to rise sooner, and to higher peak values than measured, for all the depths considered.

The possibility of improving the correlation, especially for tests 3 and 4 if the optimization method is repeated on the data of these tests individually (*i.e.* determining the self-organizing maps using data from these tests separately and then applying the determined model inputs to all the models) was investigated. The improvements obtained for tests 3 and 4 were, however, small, and for tests 1 and 2 this resulted in more severe deviations from the measured values than for tests 3 and 4 (Figure 9).

Although significant improvements are visible in Figure 9 compared with the initial default model parameters, better overall agreement between predicted and measured temperature profiles would be expected, particularly for tests 2–4. In principle, the differences can be attributed to one of three factors: (1) modelling deficiencies or errors, (2) model configuration parameters errors, or (3) experimental temperature measurement errors. With the latter being already identified as likely, the correlations between the temperature profiles might well be improved by using the same technique on test data with less measurement errors. Despite these uncertainties, the optimized model parameters (last column of Table VII) have been shown to be the best that could be determined for the test data available and with the methods described here. Thus, in order to further evaluate the performance of the model in terms of its ability to predict other key results (since temperature profile predictions are not the only important output of this model), these model parameter values are considered to be in the order of the ideal values, and subsequent models using them are used in further evaluation in the following sections.

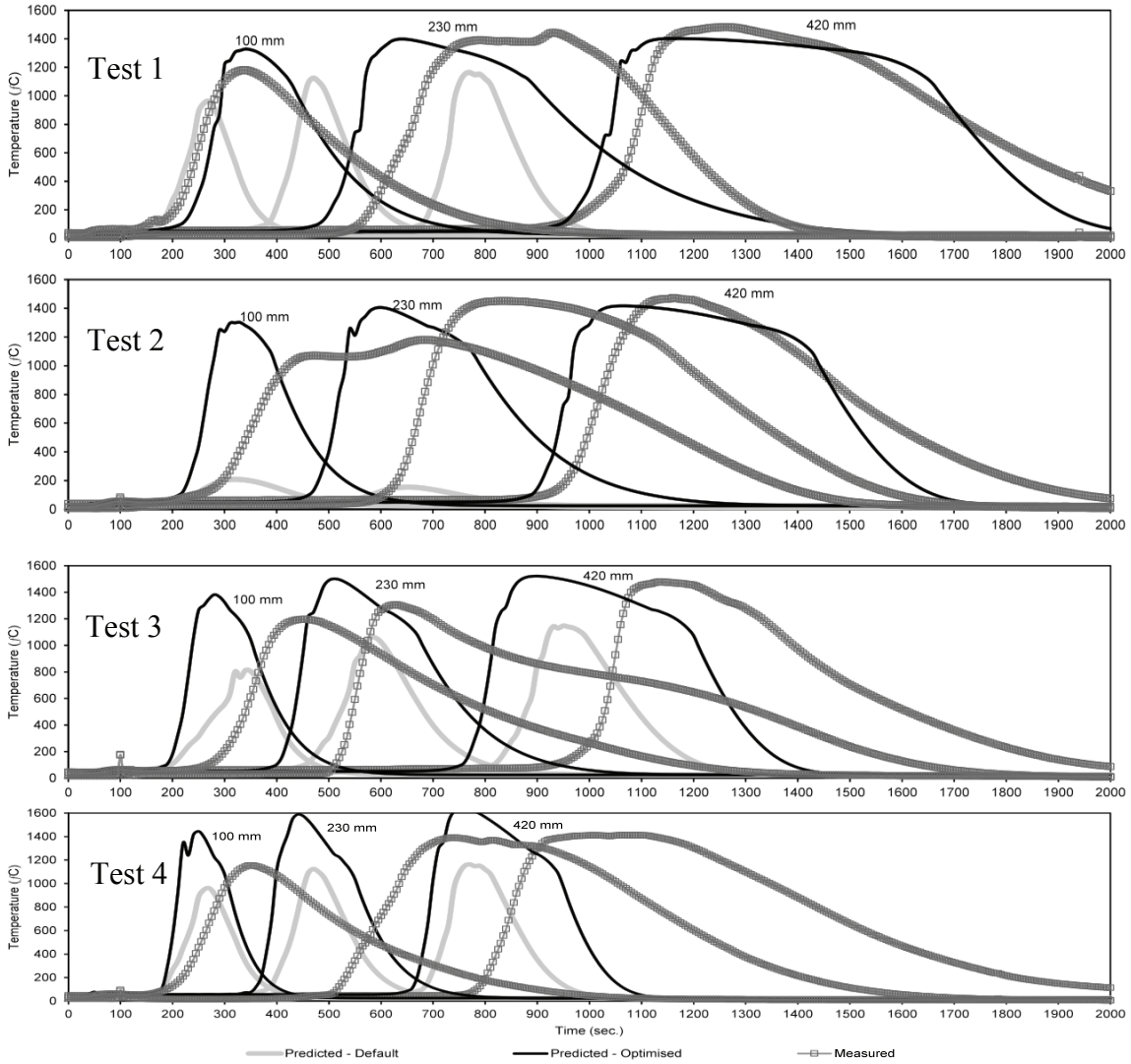

Figure 9. Predicted and measured temperatures at depths of 100, 230, and 420 mm for sinter pot tests 1 to 4 - default and optimized model parameter values used

Model results

Important result parameters are summarized in Table VIII, as derived from calculating the sinter models for each sinter test using the optimized model parameter values determined in the preceding section (last column of Table VII). It is important to note that in the model, the sintering and burn-through times are calculated using the temperature predicted for the last element at the bottom of the sinter bed, as the free space below actual sinter bed is not modelled. In the case of the model, temperatures of over 1400°C in the last element are predicted when burn-through occurs, whereas in the test data the highest temperatures achieved are typically below 600°C. Sinter performance parameters based on these temperatures measurements are therefore expected to differ slightly.

These results are compared with those calculated from the measured test data (Table II). Some result parameters are also listed in Table VIII that have been derived by averaging model result values at all the height elements at the end of the simulation. Listed are the enclosed area above 200°C, maximum fraction melted, and time above 1100°C. These parameters can be seen to vary between the four tests, and should further test work be conducted with sinter strength properties derived, correlations with these could be investigated and possibly included in the model to predict such sinter properties.

Table VIII. Summary of performance parameters determined from models representing the four sinter pot tests using optimized model parameter values

Predicted parameter	Test 1	Test 2	Test 3	Test 4
Sintering time - cool to 150°C below bed (min)	36.2	30.8	25.7	20.0
Burn-through time – max. temperature below bed (min)	30.7	26.8	21.8	17.2
Burn-through rate (mm.min^{-1})	16.3	18.6	22.9	29.1
Production rate (t.m^{-2}sinter per 24 h)	28.3	32.7	38.2	43.5
Fuel consumption rate (kg.t^{-1} sinter)	70.4	67.4	67.7	68.7
Yield (%)	85.6	85.6	86.7	86.8
Enclosed area > 200 °C - av. (min.°C)	8801	6627	5757	3918
Max. solids fraction melted - av.	0.90	0.92	0.95	0.96
Time > 1100°C - av. (s)	363.2	275.4	236.4	154.6

Correlations between the measured results (Table II) and the model-predicted results (Table VIII) are illustrated in Figure 10 and Figure 11 for some of the sintering performance parameters. The following observations are made for each of the result parameters investigated here:

- *Burn-through time (Figure 10a)*: derived as the time for the bottom of the sinter bed to reach its maximum temperature. For test 1 a significantly longer burn-through time is predicted, with good correlations for the other three tests
- *Burn-through rate (*Figure 10*b)*: derived from the burn-through time (above) and sinter bed height (including grit). Effectively, the inverse of the burn-through time is observed, with good correlation for all tests except test 1, where a significantly lower rate is predicted
- *Sinter production rate (Figure 11a)*: derived from the sintering time when the bottom of the bed has cooled to below 150°C. Good correlation obtained between predicted and measured values for all tests except test 1 where a lower production rate is predicted, which follows on from the slower sintering time predicted
- *Total fuel consumption rate (Figure 11b)*: good correlation obtained for all but test 2. Note, however, the very narrow range of the values, and possible sensitivity to inaccuracies likely to originate from the test work.

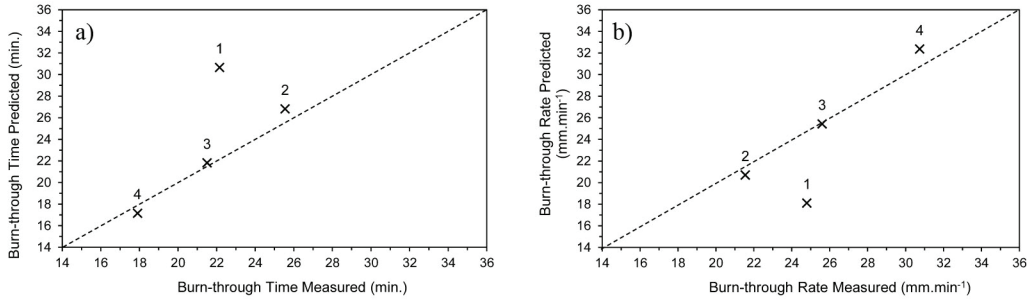

Figure 10. (a) Burn-through times and (b) rates predicted and measured in the four sinter pot tests

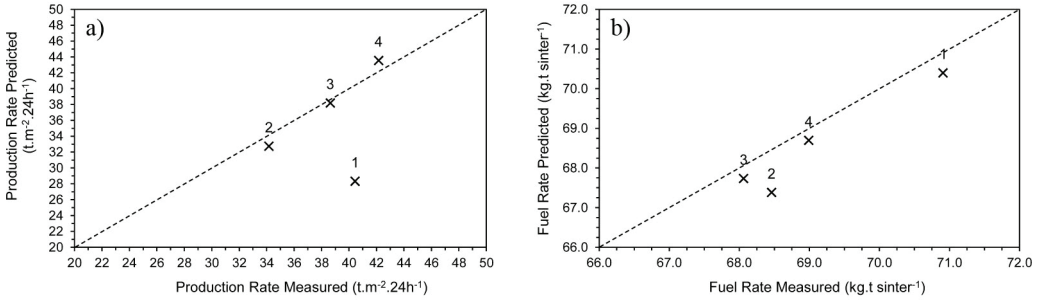

Figure 11. (a) Production rates and (b) total fuel consumption rates predicted and measured in the four sinter pot tests

Temperature measurements in the free space below the sinter bed are expected to be more consistent and less prone to experimental errors, with the thermocouples not being influenced by the high temperatures and movement in the bed as the case might be with thermocouples located within the sinter bed. The good correlations found in Figure 10 and Figure 11 are, however, better than expected, considering firstly the differences in predicted and measured temperature profiles (Figure 9), and secondly that the experimental results (Table II) are based on measurements in the free space below the sinter bed, whereas the predicted results (Table VIII) are based on temperatures for the elements at the bottom of the sinter bed. The results do, however, indicate that in most cases the model predicts that these result parameters will change in the same direction when varying input parameters, as observed in the test work. With further test work these correlations might differ in that the slope could change, and an offset could be expected between predicted and measured result parameters because of the difference in the location of the modelled *versus* the measured temperatures. It should be possible to easily compensate for the temperature lost in the free space below the sinter bed in determining the burn-through time. For example, a time factor can be added to that where the peak temperature is predicted in the last element at the bottom of the sinter bed, or by specifying a cool-down temperature value to reach to indicate burn through.

Conclusions

A model of the iron ore sintering process has been developed and solved using the finite difference method. The model was validated against results from four sinter pot tests conducted on various feed mixtures, and differences were found between predicted and measured temperature profiles. Model parameters were identified, and their values optimized by using temperature measurements from the available test data, the model, and the 'Kohonen self-organizing maps' method. The correlation between the characterization parameters of the predicted and measured temperature profiles improved notably. Appreciable differences in the temperature profiles are, however, still present, and are likely due to measurements errors in the sinter pot tests, as other authors have reported to be typical (Loo *et al*., 2012; Zhou *et al*., 2012a).

These model parameters were assumed to be the best that could be determined with the available test data and thus were treated as ideal values in further evaluation of the model. The models were calculated with these values and the sinter performance parameters found to correlate well with those from the sinter pot tests. The largest deviations were observed for test 1 (no iron ore concentrate in the feed), as a significantly slower burn-through time and rate was predicted, relating to a lower sinter production rate. The results indicate that this model correctly considers variations in the inputs, as the model results vary in the same direction and order of magnitude as the test results for the four sinter pot tests. The accuracy of the model could be further improved by re-evaluating the model and the optimization method for possible deficiencies, and then conducting further test work on a wider range of sinter feed mixtures.

It is concluded that despite likely measurement errors in the test work, the accuracy of the model needs to be further improved through optimization of uncertain model parameters and inclusion of further modelling phenomena such as bed shrinkage and its effect on bed permeability. The addition of granulation modelling would also be of great value, eliminating the need to physically perform granulation and measure the particle size and void fraction (or JPU).

References

Clixby, G. and Young, R.W. 1992. Mathematical model of the sintering process. *Proceedings of the 10th Process Technology Conference. Second International Symposium on Modeling in the Iron and Steel Industry*, Toronto, vol. 10. pp. 391-402.

Dash, I., Carter, C.E., and Rose. E. 1974. Heat wave propagation through a sinter bed; a critical appraisal of mathematical representations. *SIMAC 74: Proceedings of the Conference on Measurement and Control in the Steel Industry*, Sheffield. pp. 8/1-8/7.

Debrincat, D., Loo, C.E., and Hutchens, M.F. 2004. Effect of iron ore particle assimilation on sinter structure. *ISIJ International*, vol. 44, no. 8. pp. 1308-1317.

Kohonen, T. 2001, Self-Organizing Maps, 3rd edn. *Springer Series in Information Sciences*, vol. 30.

Lwamba, E. and Garbers-Craig, A.M. 2008. Control of the grain size distribution of the raw material mixture in the production of iron sinter, *Journal of the Southern African Institute of Mining and Metallurgy*, vol. 108. pp. 293-300.

Loo, C.E., Tame, N., and Penny, G.C. 2012. Effect of iron ores and sintering conditions on flame front properties. *ISIJ International,* vol. 52, no. 6. pp. 967-976.

Majumder, S., Natekar, P.V., and Runkana, V. 2009. Virtual indurator: a tool for simulation on induration of wet iron ore pellets on a moving grate. *Computers and Chemical Engineering*, vol. 33. pp. 1141-1152.

Mei, C., Zhou, J., Peng, X., Zhou, N., and Zhou, P. 2010. Simulation and Optimization of Furnaces and Kilns for Nonferrous Metallurgical Engineering. Springer, New York. pp. 50-52.

Patisson, F., Bellot, J.P., and Ablitzer, D. 1990. Study of moisture transfer during the strand sintering process. *Metallurgical Transactions B*, vol. 21B. pp. 37-47.

Patisson, F., Bellot, J.P., Ablitzer, D., Marliere, E., Dulcy, C., and Steiler, J.M. 1991. Mathematical modelling of iron ore sintering process. *Ironmaking and Steelmaking*, vol. 18, no. 2. pp. 89-95.

Thurlby, J.A. 1988. A dynamic mathematical model of the complete grate/kiln iron-ore pellet induration process. *Metallurgical Transactions B*, vol. 19B. pp. 103-102.

Yang, W., Ryu, C., Choi, S., Choi, E., Lee, D., and Huh, W. 2004. Modeling of combustion and heat transfer in an iron ore sintering bed with considerations of multiple solid phases. *ISIJ International,* vol. 44, no. 3. pp. 492-499.

Zhou, H., Zhao, J.P., Loo, C.E., Ellis, B.G., and Cen, K.F. 2012a. Numerical modeling of the iron ore sintering process, *ISIJ International*, vol. 52, no. 9. pp. 1550-1558.

Zhou, H., Zhao, J.P., Loo, C.E., Ellis, B.G., and Cen, K.F. 2012b. Model predictions of important bed and gas properties during iron ore sintering. *ISIJ International*, vol. 52, no. 12. pp. 2168-2176.

The Authors

Jacques Muller, *Senior Process Engineer, Metallurgy*

Following graduation from the University of Pretoria in Chemical and Process Control Engineering, I began my career in 2004 working primarily in a consulting environment on pyrometallurgical process engineering projects. Experience in applying various types of modelling techniques to analyse and optimise processes. From 2011 I have worked in a team responsible for design, commissioning and optimisation of a demonstration facility part of the Exxaro AlloyStream project, applying proprietary pyrometallurgical process technology to produce ferromanganese. I am currently completing a masters degree in metallurgy, in which taphole flow is modelled for ferromanganese and silicomanganese processes.

Tamryn de Vries, *Senior Process Engineer*, Anglo American Kumba Iron Ore

I started my career as a Graduate Metallurgist at Anglo American Platinum's Base Metals Refinery in Rustenburg where I spent 3 years (2003-2005). I then moved to Platinum's Polokwane smelter (2006-2010) where I spent 5 years in various roles including Process Metallurgist, Senior Metallurgist and finally Production superintendent (Production HOD, managing 4 shift teams plus dayshift staff). Most recently I joined Kumba Iron Ore as a Senior Process Engineer 4 years ago, where I am responsible for Value-in-Use modelling of Iron and Steelmaking processes, providing technical support in terms of pyrometallurgy expertise to Kumba's Marketing, Projects and Process Metallurgy disciplines.